66-1174

SEPTEMBER 19, 1966

SECOND QUARTERLY PROGRESS REPORT

RESEARCH STUDY ON INSTRUMENT UNIT THERMAL CONDITIONING HEAT SINK CONCEPTS

JUNE 1 TO AUGUST 31, 1966

PREPARED FOR

GEORGE C. MARSHALL SPACE FLIGHT CENTER
HUNTSVILLE, ALABAMA
CONTRACT NO. NAS8-11291

GARRETT AIRESEARCH MANUFACTURING DIVISION
Los Angeles, California

66-1174
SEPTEMBER 19, 1966

SECOND QUARTERLY PROGRESS REPORT

RESEARCH STUDY ON INSTRUMENT UNIT THERMAL CONDITIONING HEAT SINK CONCEPTS

JUNE 1 TO AUGUST 31, 1966

PREPARED FOR

GEORGE C. MARSHALL SPACE FLIGHT CENTER
HUNTSVILLE, ALABAMA
CONTRACT NO. NAS8-11291

Prepared by: D. W. Graumann
Edited by: R. A. Stone
R. A. Stone
Approved by: I. G. Austin
I. G. Austin
F. E. Carroll
F. E. Carroll

GARRETT AIRESEARCH MANUFACTURING DIVISION
Los Angeles, California

CONTENTS

FIGURES

SECOND QUARTERLY PROGRESS REPORT
RESEARCH STUDY ON INSTRUMENT UNIT
THERMAL CONDITIONING HEAT SINK CONCEPTS
JUNE 1 TO AUGUST 31, 1966

INTRODUCTION

This report reviews the work accomplished by the AiResearch Manufacturing Company, a division of The Garrett Corporation, Los Angeles, California, between June 1 and August 31, 1966, under National Aeronautics and Space Administration Contract NAS8-11291. This contract is for a research study on instrument unit thermal conditioning heat sink concepts. This report is the second quarterly progress report under the referenced contract which was signed on March 11, 1966. The previous report under this contract was issued under AiResearch report number 66-0979.

PROGRESS SUMMARY

During the second quarterly reporting period, work was performed in the following areas: Under Task I, Water Boiler Heat Sink Module, detail drawings of the wick performance test module were completed, initial units were assembled and installed in the test loop, and testing was begun. Additional metal and nonmetal wicks were ordered and wicking rate tests were initiated. Under Task II, Water Sublimator Heat Sink Module, breakthrough analysis was continued and capillary tube testing was performed to verify analytical predictions. Design of a sublimation performance test fixture was completed. Additional porous plates were procured and bench tests are about 20 per cent complete.

TASK I: WATER BOILER HEAT SINK MODULE

Wick Heat Transfer and Performance Testing

In order to determine the performance of various wick materials and configurations, wick performance test modules have been designed and assembled and are currently being tested. Modules have been designed so that the following variables might be investigated: wick material, thickness, fin configuration, wick height, wick density, heat flux, sink temperature and brazed condition. Components of a typical test module are shown in Figures 1 and 2. Figure 1 shows the electrical heater and the heavy copper plate to which it

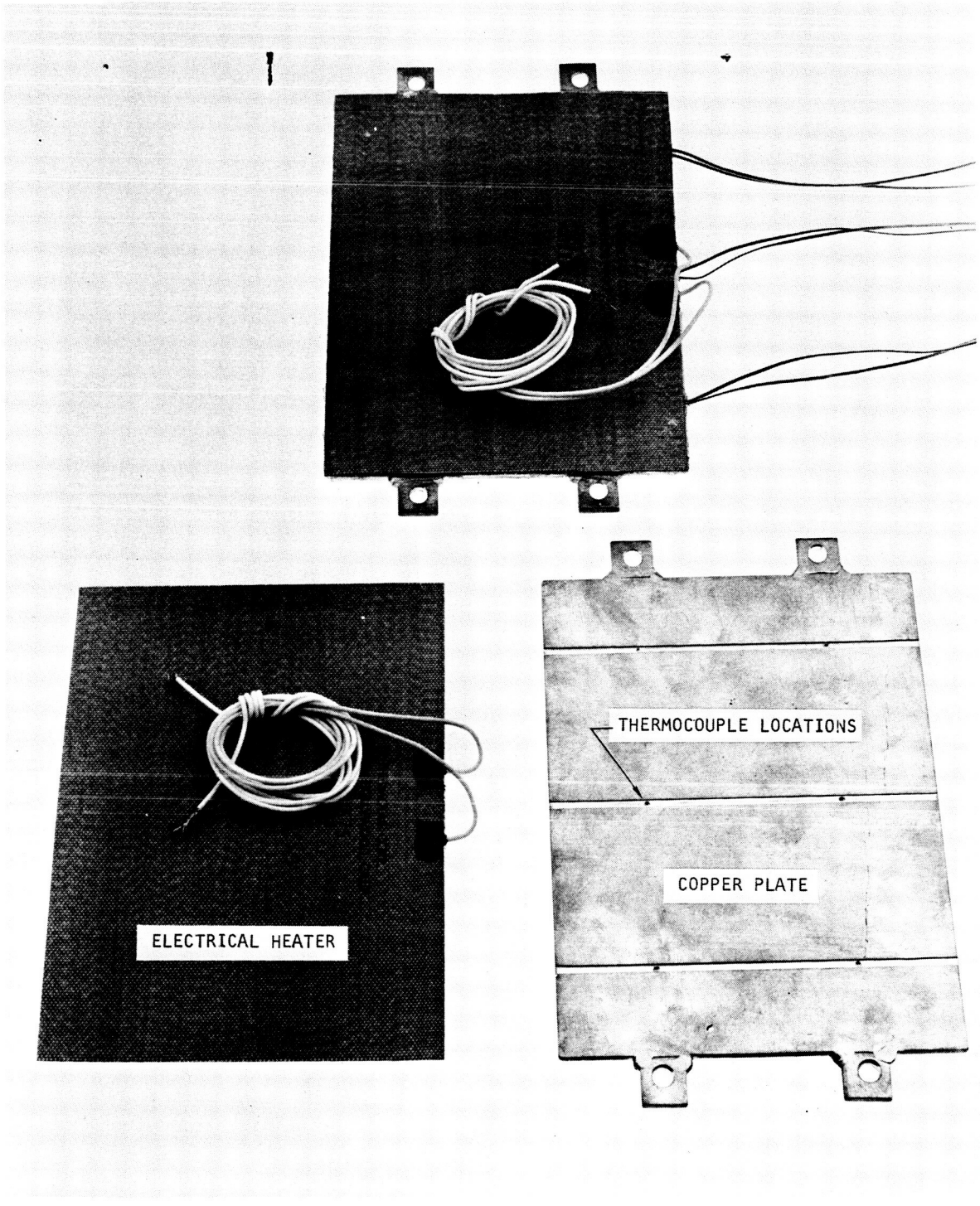

Figure 1. Wick Performance Test Module Heater Plate

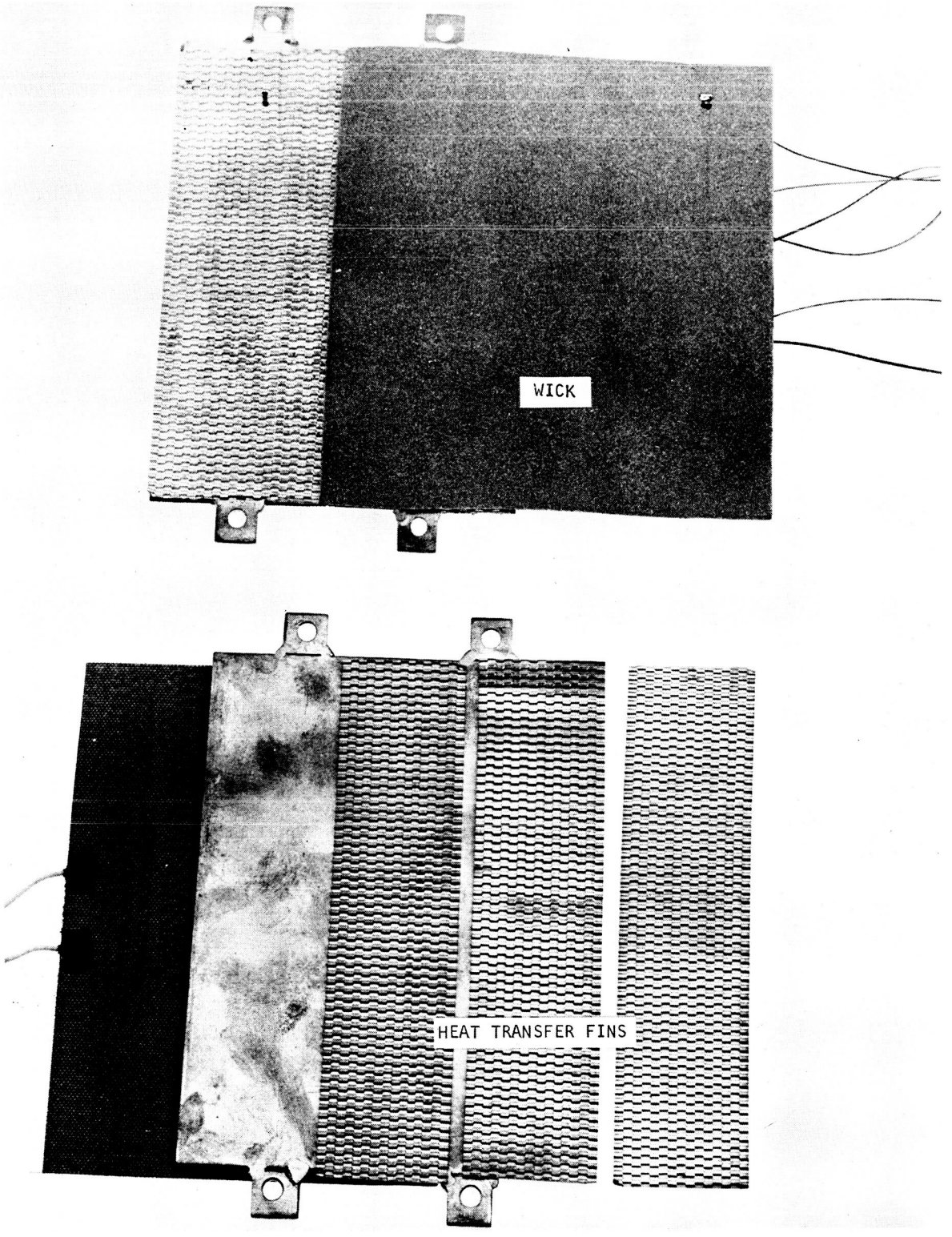

Figure 2. Wick Performance Test Module Assembly

is attached. Electrical heaters were chosen for simplicity of operation and to provide better heat balances, while the copper plates assure uniform heating and more precise definition of the temperature boundary conditions. Copper-constantan thermocouples are imbedded in the copper plate at six locations at two elevations so that the heater temperature may be recorded as a function of position. This allows for the identification of hot spots in the wicks and indicates any variation of performance with elevation. The heater is attached to the copper plate with RTV silicon rubber. Figure 2 shows the fins and wick, in addition to the heater and copper plate. The fins shown are rectangular offset; however, triangular fins also are being tested. The test modules are heated from both sides, forming a heater-plate-fin-wick-fin-plate-heater sandwich. Initial tests are being made with brazed and unbrazed wick-fin modules to determine the effect of brazing on the module performance. It is thought that brazing might assure better performance due to increased contact between the wick and the heat conducting fin, thereby eliminating any additional heat transfer resistance due to a gap between the fin and the wick surface. However, it is possible that sufficient contact may be obtained by pressure alone, eliminating any need for brazing. There might also be an adverse effect of brazing if the braze alloy wicks into the wick material and plugs it, thereby restricting liquid flow. This would, of course, be a function of the amount of braze alloy required to obtain a good braze joint. Once the relative merits of brazed and unbrazed configurations have been determined, the performance of rectangular and triangular fins will be compared. Details of further testing will depend to some extent upon the results of the initial tests; however, it is anticipated that the following range of variables will be covered.

Wick thickness will be varied from 0.030 inches to 0.250 inches. Previously performed wicking height tests reported in the first quarterly report showed a strong dependence on wick thickness. It is anticipated, therefore, that wick thickness may have a definite effect upon the heat transfer performance characteristics of a particular material. This would be expected, especially at high heat fluxes, when the ability of a thin wick to deliver sufficient water may become limiting. It should be mentioned here that the reason for the dependence of wicking rate upon the wick thickness is not fully understood at this time; however, additional wicking rate tests are planned

to solve this problem, as explained below. Heat fluxes will range as high as possible without exceeding the temperature limitations of the test assembly. Test modules of 1.5, 3, 4.5, and 6-inch heights have been assembled so that the effect of wick height might be determined. Wick densities will range from 10 to 30 per cent and wick materials available for testing are stainless steel, nickel, copper, and silica vitreous fiber. Additional materials may be tested as a result of the wicking height tests.

A schematic of the test setup is shown in Figure 3 and photographs in Figures 4 and 5. The wick module is enclosed in a bell jar so that the boiling temperature may be controlled by reducing the pressure. Separate power input is supplied to each heater plate and individual voltmeters, ammeters and variacs are provided. The water from the supply tank is filtered through a 1/2μ absolute Millipore filter, and metering is provided for extended duration testing. The test section is wrapped with multiple layers of aluminized Mylar to reduce the heat losses.

Initial tests have been run to verify the workability of the system. Tests with no water are currently underway to calibrate the system for heat leak. For each run, the 12 heater temperatures are recorded, as well as the current, voltage, and bell jar pressure. Data is taken at ten minute intervals to assure that steady state has been reached at each heat flux.

A computer program has been written to facilitate reduction of wick boiler test data. The basic inputs are the test module dimension, the steam chamber pressure, the input voltage, the input current, and the local plate temperature. This data is recorded on special forms and punched directly from them onto input data cards. The program calculates a local and an average heat transfer coefficient h, defined as $h = \frac{Q}{A(T_h - T_s)}$ where:

Q = heat input to plate

A = heater plate area

T_h = local heater temperature

T_s = boiling temperature

The boiling temperature is assumed equal to the saturation temperature corresponding to the chamber pressure. A wall heat transfer conductance can be used to include a metal plate temperature drop between the thermocouples and the water side surface of the plate.

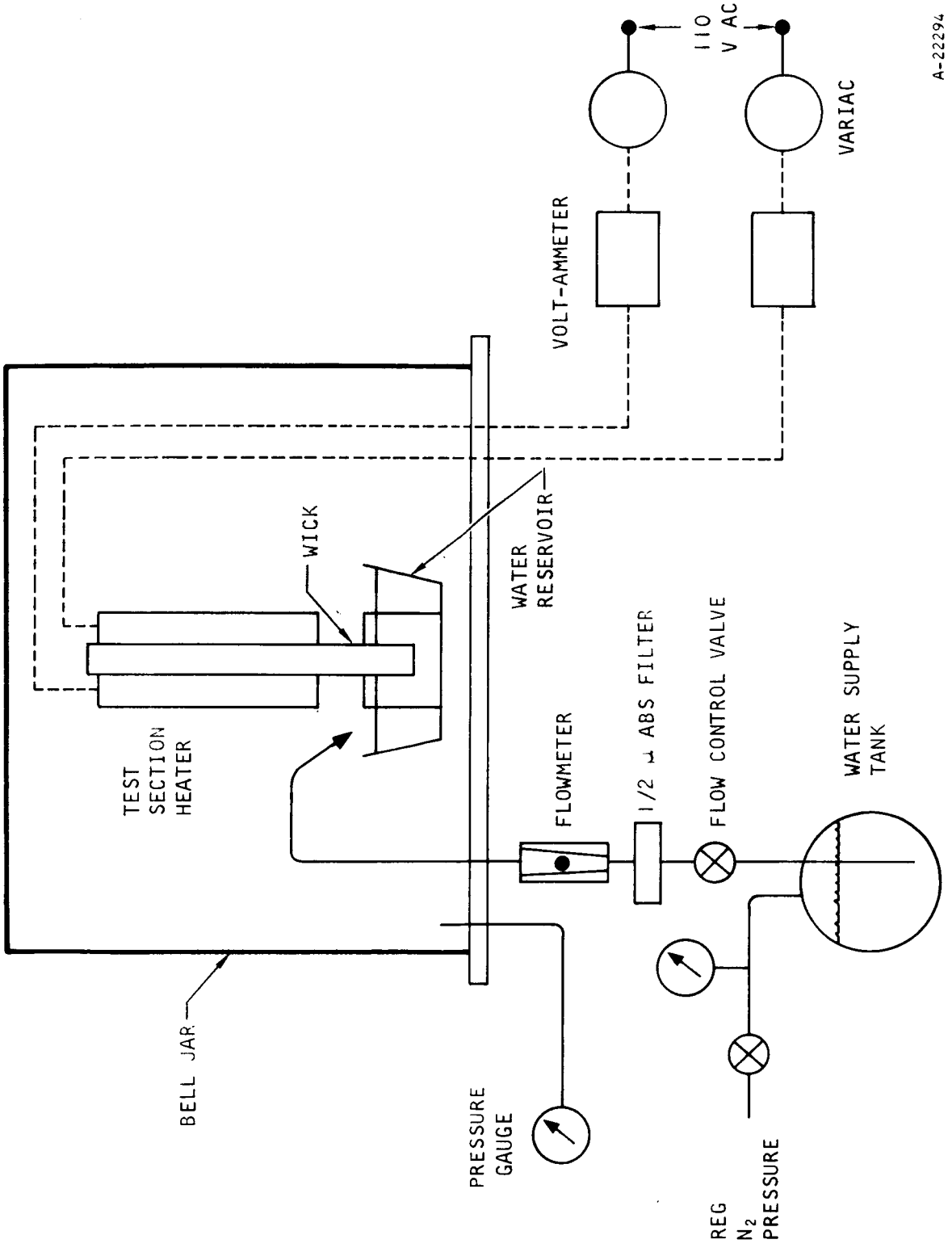

Figure 3. Wick Heat Transfer Performance Test Setup

F-6004

Figure 4. Single Wick Boiler Module

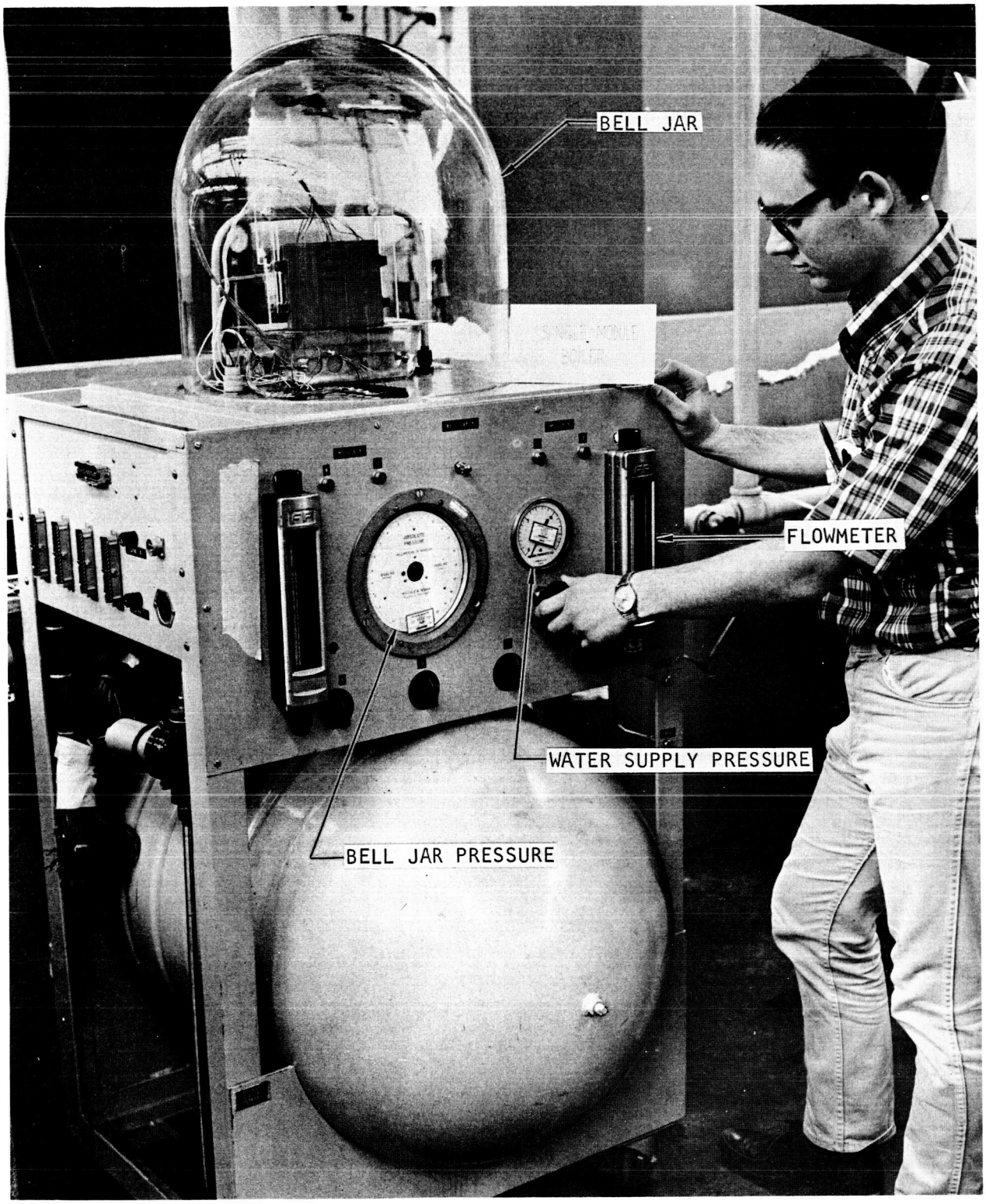

F-6003

Figure 5. Single Wick Boiler Module Test Setup

Wicking Height Tests

The first quarterly progress report included results of previous wick rate tests performed at AiResearch. These tests were run before it was fully appreciated how easily susceptible wicks are to contamination and how extreme is the requirement for cleanliness. Therefore, wick rate tests are being repeated under more carefully controlled environmental conditions. Three basic tests are included in this series, vertical rise time, horizontal advance time, and wick water retention. The vertical rise time test involves mounting the wick specimens in a vertical position and immersing the bottom end of the wicks in water. A clock is started at the moment the wick is immersed and water level in the wick is recorded at regular time intervals. Visual observations are supplemented by attaching litmus paper strips to the wicks. In the horizontal advance tests, the specimens are mounted in a horizontal position and water feed is accomplished by using pieces of cellulose sponge to wet the bottom portion of the wick. Data is recorded in the same manner as in the vertical rise tests. In the wick water retention test, after the dry weight of the specimen has been determined, the wick is immersed in water until it is thoroughly wet. It is then removed and hung in a vertical position until dripping has essentially ceased, and the wet weight of the wick is determined.

In order to assure cleanliness of the test specimens, the following precautions are being observed:

1. All testing will be conducted in the AiResearch Altitude Laboratory Clean Room.
2. All specimens will be thoroughly cleaned prior to testing.
3. Wick specimens will be kept in nylon bags when not in use.
4. Wicks will be handled only with tongs or clean rubber gloves.
5. Only distilled 1/2 micron filtered water will be used in testing.

TASK II: WATER SUBLIMATOR HEAT SINK MODULE

Breakthrough Analysis

1. Experimental Verification of Analytical Breakthrough Predictions

An analysis of liquid and vapor breakthrough was presented in the previous quarterly report. The effects of contact angle and pore exit sharpness were investigated, and the analytical results are shown in Figure 6 in the

form of normalized breakthrough pressure vs. contact angle. Tests were initiated in order to verify the analytical predictions.

The test apparatus for liquid and vapor breakthrough is shown in Figure 7. Stainless steel capillary tubes of known inside diameter were used and were thoroughly cleaned prior to testing. The liquid breakthrough test involved gradually increasing the liquid head and observing the pressure differential at which breakthrough occurred. In the vapor breakthrough test, the gas pressure was slowly increased until the first dynamic bubble appeared from the test fluid.

The tests conducted to date were performed with water and mercury for sharp cornered capillary tubes in order to verify the $\rho/R = \infty$ curve in Figure 6. With these fluids, results were obtained for a wetting ($\theta < 90^0$) and a nonwetting ($\theta > 90^0$) liquid.

The results of these initial tests are shown in Figure 6. It is seen that fairly good agreement with the analytical predictions was obtained. The normalized gas breakthrough pressures are within a couple per cent of the predicted values while the liquid breakthrough pressure of mercury is about ten per cent less than the analytical prediction. A possible explanation of this might be the value used for the interfacial surface tension of mercury and air. Perry[1] states that the surface tension of mercury is "variable and decreases with time," which could explain the discrepancy. The contact angle of water with stainless steel is shown as a range rather than a point because of the difficulty in determining its exact value. Observation under moderate magnification of the liquid drops on the test apparatus during testing, as well as the protruding liquid-vapor interface, indicated a contact angle in the neighborhood of 30^0. Photographs of water drops on a stainless steel plate were made in order to obtain a more accurate value of the contact angle; however, this was unsuccessful due, probably, to contamination of the plate between cleaning and photographing, and contact angles ranging from 30^0 to 90^0 were obtained. The literature gives contact angles of water on "cleaned" stainless steel surfaces of from 0^0 to 42^0, depending on the cleaning procedure and whether the contact angle is the advancing or receding angle.

---

[1] Perry, John H., Chemical Engineers Handbook, 3rd Edition, 1950, McGraw-Hill Book Company, Inc., pg. 363.

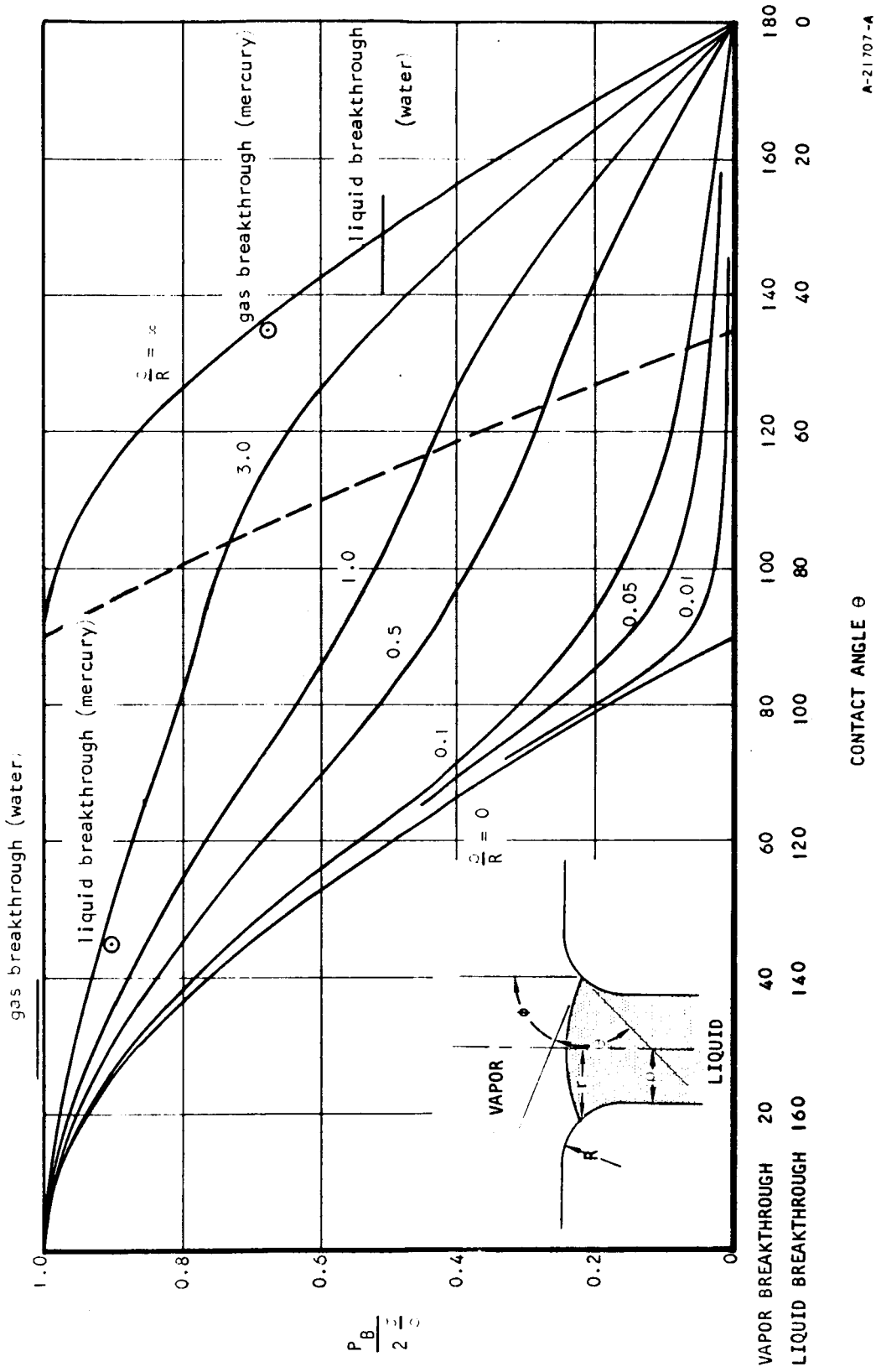

Fig. 6. Normalized Breakthrough Pressure as a Function of Contact Angle and Exit Sharpness

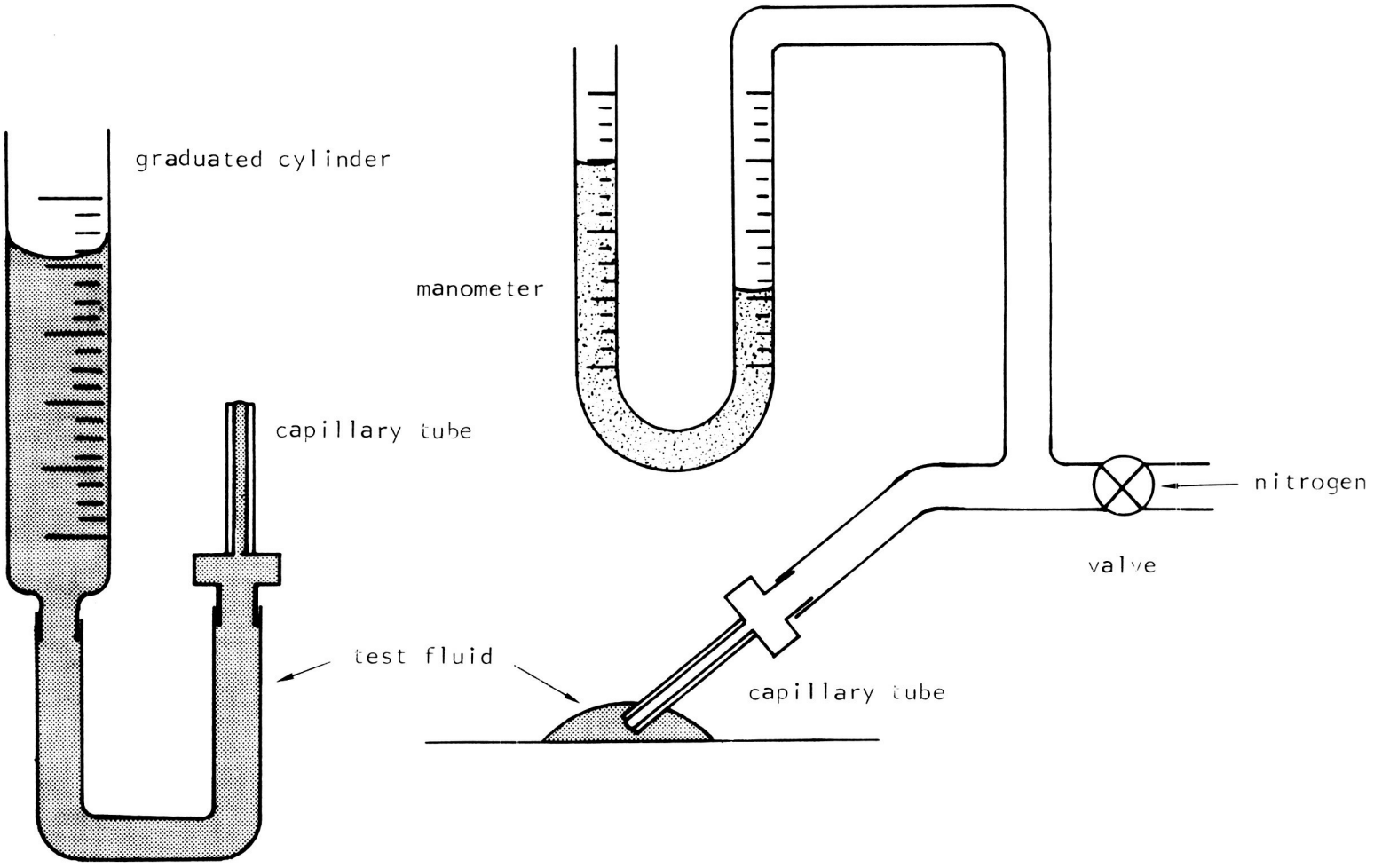

Figure 7 Breakthrough Test Apparatus

2. Effect of Pore Exit Sharpness on Breakthrough Pressure

As stated in the previous analyses of breakthrough phenomena, the breakthrough pressures for a given system are a function of the surface tension, the pore diameter, the contact angle, and the exit sharpness ratio (the ratio of the pore radius to the radius of curvature of the pore exit). These system variables can all be important and, therefore, all three must be considered when investigating breakthrough.

It has been generally assumed that the smaller the pore diameter in a porous plate, the larger the liquid breakthrough pressure. However, it can be shown from Figure 6 that this is not necessarily true, since the pore exit sharpness can have a pronounced effect. For instance, the normalized liquid breakthrough pressure for a contact angle of 40^0 for a pore with an exit sharpness ratio of 1.0 of 5.5 times that for one with a sharpness ratio of 0.1. This means that the pore with the sharper exit can be up to 5.5 times larger than the pore with the dull exit and still have a higher breakthrough pressure. A sketch of this condition is shown below where for a contact angle less than 50^0, the larger pore has a higher liquid breakthrough pressure than the smaller, even though the diameter is five times greater.

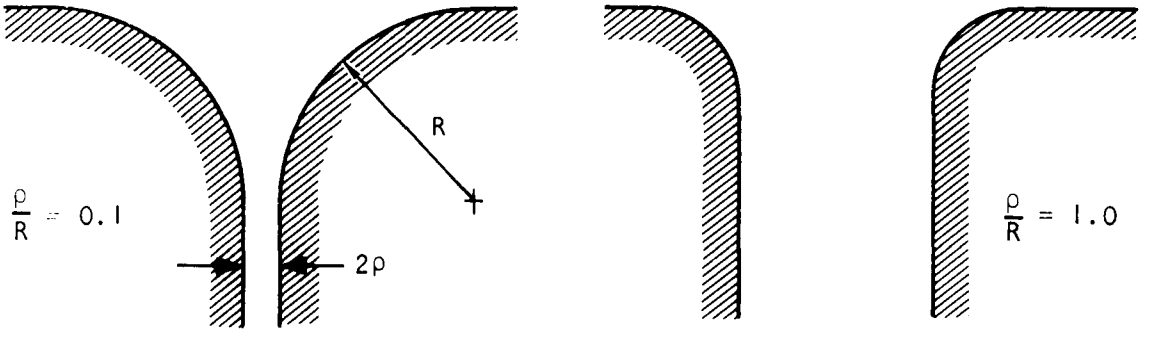

Stated another way, for a contact angle of less than 50^0, the liquid breakthrough pressure obtainable at sharpness ratios of 1.0 and 0.1 are 1/2 and 1/11 of that obtained with an absolutely sharp pore ($\rho/R = \infty$) as indicated in Figure 6. Obviously then, a sharp pore exit (large $\frac{\rho}{R}$) is desirable in porous plates for sublimator applications. It is possible to determine experimentally an equivalent pore exit sharpness of a porous plate. This was done

for porous plate data taken in this study and is reported below.

Another problem which the effect of pore exit sharpness brings to light is the matter of porous plate specifications. If a higher liquid breakthrough pressure is desired, it may not be sufficient to specify merely a smaller pore diameter (higher bubble point or gas breakthrough pressure), for it has been shown than this does not guarantee a higher liquid breakthrough pressure since exit sharpness may vary. Therefore, it appears necessary to specify the liquid breakthrough pressure in some manner, and this is being studied at this time in order to develop meaningful and complete engineering specifications for porous plates.

3. Effect of Contact Angle on Breakthrough Pressure

The liquid breakthrough pressure may also be increased by increasing the contact angle as seen from Figure 6. A larger θ increases the breakthrough pressure in two ways. First, it reduces the adverse effect of a small exit sharpness as seen by the fact that liquid breakthrough curves for the different exit sharpness ratios move closer together as θ increases. For example, at $\theta = 40^0$, the normalized breakthrough pressure for an exit sharpness of 0.1 is less than 20 per cent of that for $\rho/R = 1.0$, whereas at $\theta = 140^0$, the breakthrough pressure of the duller pore is equal to about 80 per cent that of the sharper pore. Secondly, the stronger dependence on cosine θ for $\theta > 90^0$ causes the breakthrough pressure to increase. This is illustrated by the fact that in changing the contact angle from 40^0 to 140^0, the magnitude of the liquid breakthrough pressure increases by a factor of 3 for $\rho/R = 1.0$.

Whereas it may not be possible to vary the exit sharpness of a porous plate without going into an elaborate plate development program, it would be possible to vary the contact angle to increase the breakthrough pressure. By treating the plate or the subliming fluid, a contact angle of greater than 90^0 could be obtained. The literature cites water contact angles of $\sim 100^0$ on stainless steel plates contaminated with stearic acid, oleic acid, paraffin oil, or naphthenic oil. This large contact angle makes these compounds possible candidates for use in porous plates; however, since no study or testing of these compounds has been performed as yet, it is not known at this time if they would prove satisfactory. Such questions as how the surface tension of water is affected by them and how permanently they adhere to a surface must be answered before they can be seriously considered. Another possibility would be Teflon

coating of metal porous plates, or even porous Teflon plates. Contact angles of about 110^0 are obtainable for water on Teflon. Some Teflon plates have been tested for breakthrough pressures and the results are reported below.

Porous Plate Bench Tests

An AiResearch Engineering Work Order describing the porous plate bench tests was included in the previous quarterly report. A number of these test have been performed on the sample porous plates listed below:

	Material	Supplier
1.	Teflon - sintered particles	Aircraft Porous Media
2.	KEL-F - sintered particles	Aircraft Porous Media
3.	Rigimesh - woven and sintered nickel metal wire	Aircraft Porous Media
4.	nickel - sintered particles	Lockheed

The initial test performed on each sample is the bubble point (or gas breakthrough) in alcohol. The alcohol bubble point is defined as the pressure at which the first dynamic bubble appears on the surface when the back side of the plate is pressurized and the surface is covered with a thin layer of 95 per cent solution of ethanol. From this test one may determine the maximum equivalent pore diameter of the plate. Since alcohol forms a contact angle of essentially zero degrees with most surfaces, the bubble point pressure is dependent only upon pore size and surface tension, not upon exit sharpness ratio as shown in Figure 5. Therefore, since $\frac{P_V}{2\sigma/\rho} = 1.0$ for zero contact angle, once the bubble point P_V is determined experimentally, the equivalent pore radius ρ may be determined. Since it is not known whether the pore is of circular cross-section, ρ is defined as the radius of a circular pore which would have an equivalent breakthrough pressure.

Because it is desirable to know how uniform a porous plate is with respect to pore size, a measure of the uniformity may be determined by increasing the pressure until either a certain percentage of the surface is covered with bubbles or a specific successive bubble point is reached; for instance, the tenth bubble point. In this way, by using the same equation, $\frac{P_V}{2\sigma/\rho} = 1.0$, one may

determine that a certain number or percentage of the pores is larger than a specific value. Whether a percentage or a specific successive bubble point should be determined depends to some extent upon the plate being tested. If the pore size is fairly uniform, it would probably be best to use a percentage value (usually 80 per cent) since the 10th bubble point would be quite close to the first and it becomes increasingly difficult to keep track of successive bubble points higher than 10. A specific bubble point would be desirable if the plate appeared to be quite nonuniform with respect to pore size.

Once the range of pore sizes has been determined, it is advantageous to have an idea of the shape of the pore exit, the equivalent exit sharpness ratio. The reason this is important is because of the pronounced affect it has on the liquid breakthrough pressure, a primary consideration in sublimators. The equivalent exit sharpness ratio can be determined by performing a bubble point (gas breakthrough) in water and a water breakthrough test on the sample plates. With these two breakthrough pressures, one may determine the nondimensional breakthrough pressures, $\frac{P_B}{2\sigma/\rho}$, using the pore radius determined in the alcohol bubble point test. Since these two tests are performed one after the other using the same fixtures and water supply, it can be assumed that the contact angle in each test is equal. Therefore, one may determine from Figure 6 the exit sharpness which gives the appropriate nondimensional breakthrough pressures at equal contact angles. For instance, consider a metal porous plate with an equivalent pore radius of 5 μ determined from a bubble point in alcohol test, for which gas breakthrough and liquid breakthrough pressures in water of 63 and 10 inches of water, respectively, are obtained. Nondimensional breakthrough pressures of 0.55 and 0.087 are calculated (σ_{water} = 72 dynes/cm). From Figure 6, it is seen that the exit sharpness ratio and contact angle which give these two values are 0.1 and 60^0, respectively. The contact angle of 60^0 indicates that the plate was slightly contaminated during the test, for θ is usually 30^0 or less on a clean metal surface.

An important assumption upon which this approach of finding the exit sharpness is based is that gas breakthrough in alcohol, gas breakthrough in water, and water breakthrough all occur at the same size pore. Gas breakthrough in alcohol will always occur at the largest pore; however, it has been shown previously that for a contact angle $\theta > 0^0$, breakthrough is dependent

upon the exit sharpness ratio. Therefore, it is quite possible that bubble point in water and water breakthrough might occur at pores which are smaller and less sharp than the largest pore. This can make a difference in calculating the exit sharpness if the exit sharpness of the smaller pore is significantly less than that of the alcohol bubble point pore; an analysis discussing this difference is given in Appendix 1.

With these three relatively simple breakthrough tests, it is possible to obtain a fairly precise description of the geometric characteristics of a porous plate. This was done for the porous plates listed above and the results are given below:

Teflon, KEL-F, and Rigimesh Porous Plates. Two porous Teflon specimens, two porous KEL-F samples, and one Rigimesh plate were tested and the test results are tabulated in Table 1.

It is observed that for both Teflon samples, the 10th bubble point is quite near the initial bubble point, indicating a high degree of uniformity in pore size. The maximum equivalent pore diameters of samples A and C are 20.6 and 9.4 microns, respectively. The normalized gas breakthrough pressure for these samples is seen to be quite small and the normalized water breakthrough pressure quite large. This is expected, however, since the contact angle of water with Teflon is large. The exit sharpness ratios obtained for both samples are $\frac{\rho}{R} = 0.1$ at a contact angle of $\approx 160^0$.

Some question arises as to the validity of a contact angle as large as 160^0 since values of contact angle of water on Teflon in the literature usually range close to 110^0. Observations in the laboratory of the water on Teflon contact angle ranged from 110^0 to 135^0. It does seem reasonable to expect a contact angle greater than 110^0 in the water breakthrough test because the liquid is being forced out of the pores and the characteristic contact angle would be the advancing contact angle. It is possible, as stated above, that water breakthrough and bubble point in water occurred at smaller pores with duller exits and not at the largest pore found by alcohol bubble point tests. This would cause the calculation of erroneous normalized breakthrough pressures giving θ larger than the actual contact angle. If a contact angle of 135^0 is assumed, a water breakthrough pore diameter of 7.1μ is obtained and an exit sharpness ≈ 0.03. The significance of the difference in pore diameter and exit sharpness ratio is discussed in Appendix 1.

TABLE I. POROUS PLATE TEST DATA

	Teflon Plate A	Teflon Plate C	KEL-F Plate B	KEL-F Plate D	Rigimesh Plate
Initial bubble point in alcohol, in. H_2O	17.0	37.2	3.3	3.0	66
Tenth bubble point in alcohol, in. H_2O	18.6	37.8	4.0	3.7	77
Initial bubble point in water, in. H_2O	1.8	3.4	3.7	2.0	20.5
Water breakthrough, psi	1.95	4.1	.24	.20	1.6
Maximum equivalent pore diameter, microns	20.6	9.4	106.0	118.0	5.3
Tenth largest equivalent pore diameter, microns	18.8	9.2	87.0	96.0	4.5
Normalized gas breakthrough, $\frac{Pv}{2\ \sigma/\rho}$	.03	.03	.34	.20	.093
Normalized liquid breakthrough, $\frac{P_L}{2\ \sigma/\rho}$	.95	.92	.60	.54	.20
$\frac{\rho}{R}$	$\approx$0.1	$\approx$0.1	$\approx$0.5	$\approx$0.2	$\approx$0.04
Contact angle, θ	$\approx 160^0$	$\approx 160^0$	$\approx 110^0$	$\approx 110^0$	$\approx 96^0$

As indicated, the particular KEL-F plates tested had very large pores, on the order of 100μ which would appear to be too large to permit their use as sublimator porous plates. However, the large contact angle indicates that plates of the same material but with smaller pores might be acceptable. The exit sharpnesses obtained were quite large as compared to the Teflon plates; however, this was expected since the pores were larger. For porous plates made from given-sized particles, as the pore size σ becomes smaller, the exit sharpness ratio σ/R obviously becomes smaller.

One woven wire plate, Rigimesh, was submitted to the initial series of bench tests. Fairly small pores were obtained for this sample, as well as good pore uniformity. The pore uniformity is expected because Rigimesh, which consists of multiple layers of woven wire mesh made rigid by rolling and furnace bonding, by its very composition is supposed to possess a high degree of uniformity. Photomicrographs of this material at 50 and 250 times magnification are shown in Figure 8, which further illustrates this characteristic.

Again, a small exit sharpness ratio was obtained, a characteristic which seems to be inherent in plates with small pore size. In the sintered particle and wire type of porous plate, this will always be expected as long as the particles which make up the solid portion of the plate are substantially larger than the pores and have quite rounded corners. The large contact angle indicates that the plate was contaminated.

Additional tests are planned for other Rigimesh samples with smaller pore size:

Lockheed Sintered Particle Porous Plates

Four plates were received from Lockheed and bubble point in alcohol and nitrogen permeability tests were performed on them. Bubble point in water and water breakthrough tests are currently being performed on these plates.

	Plate 1	Plate 2	Plate 3	Plate 4
Initial bubble point in alcohol, psi	14.8	14.4	13.4	14.7
Maximum pore diameter, microns	.86	.88	.95	.86

Of all the plates tested to date, these have the smallest pore diameter. Permeability tests indicate that they are also quite permeable, and these permeability results will be included in the next monthly report after additional

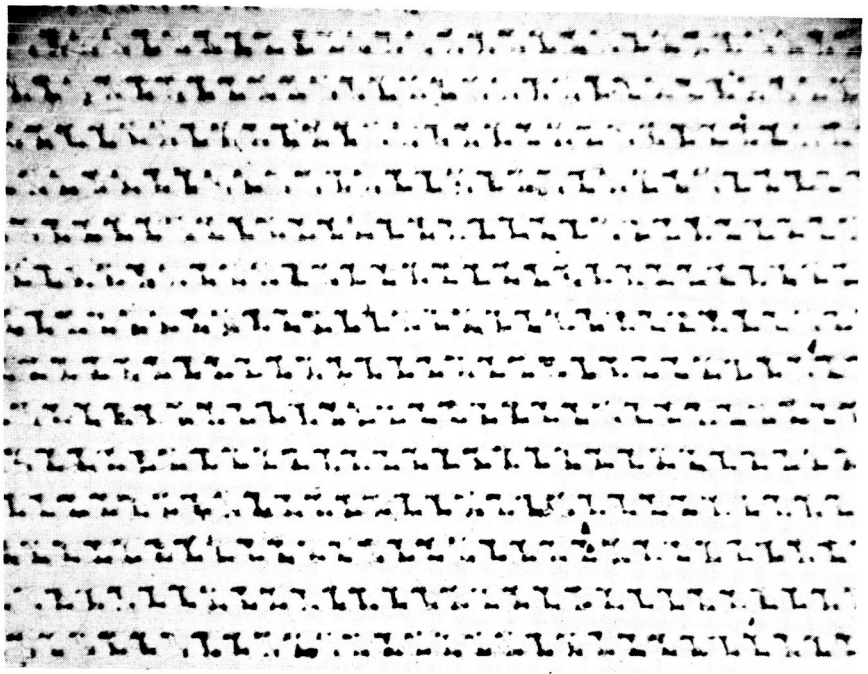

50X

250X

F-5577

Figure 8. Photomicrographs of "Rigimesh"

data on other plates is obtained so that comparisons might be made.

FUTURE ACTIVITIES

During the next quarter it is planned to continue on with the previously presented development plan. No changes are contemplated. Specific areas to be covered for each phase of the program are outlined below:

Water Boiler Heat Sink Module

1. Basic capillary and wicking analyses will be continued.
2. Controls analyses including water feed control and distribution will be started.
3. Single module testing designed to establish optimum wick characteristics will be completed.
4. Wick rate tests will be completed.

Sublimator Heat Sink Module

1. Porous plate bench tests will be completed, allowing the selection of optimum specimens for sublimation performance testing.
2. Breakthrough analysis will be continued with emphasis on methods of increasing liquid breakthrough pressure.
3. Testing of single porous plates now on hand using an electrical heat source will be completed. This series of tests is designed to relate sublimation performance to previously established bench test characteristics such as initial bubble point and nitrogen permeability.

Thermal Panel Development

1. Conceptual design studies are planned for the next quarter.

APPENDIX I

By assuming that the bubble point in water and water breakthrough occur at the same sized pore as bubble point in alcohol (i.e., at the largest pore), it is possible to determine the equivalent pore exit sharpness ratio as explained in the text. However, it has been shown that for a contact angle greater than 0, bubble point and water breakthrough may occur at a smaller pore, providing this smaller pore has a sufficiently small exit sharpness ratio. Therefore, if this is the case, erroneous values of normalized breakthrough pressure will be calculated resulting in erroneous values of contact angle and exit sharpness.

For example, consider a porous plate with two characteristic pore sizes and exit sharpness ratios; 10 μ radius holes with exit sharpness ratio of 1.0 and 5 μ radius holes with exit sharpness ratio of 0.2. An alcohol bubble point test would indicate the maximum pore radius to be 10 μ. The bubble points in water (assuming $\vartheta = 30^0$ for a clean metal plate) for the 10 μ and 5 μ radius holes are:

$$P_{V_{10}} = \left[\frac{P_V}{2\ \sigma/\rho}\right]\left[\frac{2\sigma}{\rho}\right] = [.93]\left[\frac{(2)\ (.0049\ lb/ft)}{(10\ \mu)(3.28\times10^{-6}\ ft/\mu)(144\ in^2/ft^2)}\right] = 1.93\ psi$$

$$P_{V_5} = [.89]\left[\frac{(2)\ (.0049\ lb/ft)}{(5\ \mu)\ (3.28\times10^{-6}\ ft/\mu)\ (144\ in^2/ft^2)}\right] = 3.70\ psi$$

The water breakthrough pressures for the 10 μ and 5 μ pores are:

$$P_{L_{10}} = \left[\frac{P_L}{2\ \sigma/\rho}\right]\left[\frac{2\sigma}{\rho}\right] = [.25]\left[\frac{(2)\ (.0049\ lb/ft)}{(10\ \mu)\ (3.28\times10^{-6}\ ft/\mu)(144\ in^2/ft^2)}\right] = .72\ psi$$

$$P_{L_5} = [.09]\left[\frac{(2)\ (.0049\ lb/ft)}{(5\ \mu)\ (3.28\times10^{-6}\ ft/\mu)(144\ in^2/ft^2)}\right] = .38\ psi$$

Therefore, bubble point in water would occur at 1.93 psi at the 10 μ hole and water breakthrough would occur at .38 psi at the 5 μ hole. The experimental data obtained would not indicate the hole at which breakthrough occurred, only the breakthrough pressures 1.93 and .38 psi. Therefore, assuming breakthrough occurred at the largest (10 μ) hole, one would calculate:

$$\frac{Pv}{2\,\sigma/\rho} = \frac{1.93}{(2)\ (.0049)/(10)(3.28\times10^{-6})(144)} = .93$$

$$\frac{P_L}{2\,\sigma/\rho} = \frac{.38}{2\ (.0049)/(10)(3.28\times10^{-6})(144)} = .18$$

and, from Figure 6, would obtain $\theta \approx 28^0$ and $\frac{\rho}{R} \approx 0.6$. The conclusion would be that the plate is characterized by a largest pore of 10 μ radius with an exit sharpness ratio of 0.6. The difference in exit sharpness of 40% would be of no consequence if a contact angle of $\approx 30^0$ were always maintained, because a 10 μ pore with $\frac{\rho}{R} = 0.6$ and a 5 μ pore with $\frac{\rho}{R} = .2$ have the same breakthrough pressure at $\theta = 30^0$. However, if one desired to increase the contact angle by treating the plate and tried to predict at the new θ, the new breakthrough pressure based upon a 10 μ radius pore with $\frac{\rho}{R} = 0.6$, discrepancies between the predicted and actual breakthrough pressures would occur.

It should be noted that in plates composed of spherical particles of about the same size, when the pore size is reduced by half, the exit sharpness ratio is reduced by half, since R is constant. This reduction will have no effect on the breakthrough pressure because in order for breakthrough to occur at a smaller pore, the exit sharpness must be reduced by a greater amount than the pore diameter. (In the example considered, the pore diameter was reduced by 1/2 and the sharpness ratio by 1/5.) Therefore, for plates of uniform sized particles, breakthrough at smaller pores is not anticipated. Nevertheless, it appears advisable to perform water breakthrough and water bubble point tests at contact angles near those anticipated in use.

Regardless of the uncertainties in this method, it does give a fairly good estimation of the exit sharpness ratio of a particular specimen. The tests performed so far have indicated very small (<0.1) sharpness ratios for plates with small pores (<5 μ). This is expected because of the relatively large size of the particles used in the porous plates. This small exit sharpness ratio is basically what causes clean metallic porous plates to have such low water breakthrough pressures, and two approaches are being used to solve this problem. The first has been mentioned in the text, namely reducing the effect of the sharpness ratio by going to large contact angle systems.

This will be achieved by coating the plate with a hydrophobic agent. The second is obtaining plates composed of either very small particles or sharp cornered particles, thereby increasing $\frac{\rho}{R}$.